Kingdom of Saudi Arabia

Al-Imam Muhammad Ibn Saud Islamic University

College of Sciences

Department of Physics

Impact of Substituting Ce_2O_3 with Nd_2O_3 in PVA-Ce_2O_3 Composites on Radiation Shielding Efficiency

A graduation project submitted to the Department of Physics in partial fulfillment of the requirements for the degree of Bachelor of Science in Applied Physics

by

Abdullah Dhubayrah

Supervisor

Pro. Dr. Ahmed M. El-Khayatt

AIMISIU/COS/DOP/

Riyadh- KSA- 144630 H. - 2025

Table of Contents

List of Figures

الإهداء

الشكر

ملخص عربي

تدرس هذه الدراسة تأثير استبدال أكسيد السيريوم (Ce_2O_3) بأكسيد النيوديميوم (Nd_2O_3) في مركبات قائمة على البولي فينيل الكحول (PVA) على خصائصها الهيكلية والبصرية وخواص الحماية من الإشعاع. تم تحضير أربعة أفلام مركبة باستخدام طريقة الصب المحلولي، مع تراكيز أكسيد النيوديميوم التي تتراوح بين 0 إلى 7.5 وزن٪. أظهرت النتائج انخفاضًا كبيرًا في الكثافة

بنسبة 90.81٪ للعينة التي تحتوي على أعلى تركيز من(PCNd-75) Nd_2O_3 ، ويعزى ذلك إلى زيادة الترابط التساهمي للبوليمر وانخفاض كفاءة التعبئة. تحسنت أداء الحماية من أشعة غاما بشكل ملحوظ، حيث زادت معاملات التوهين الكتلي بنسبة 665٪ عند طاقة 0.08 ميغا إلكترون فولت و11٪ عند 2.614 ميغا إلكترون فولت، ويُعزى ذلك إلى العدد الذري الأعلى لأكسيد النيوديميوم (Z = 60) مقارنة بأكسيد السيريوم .(Z = 58) ومع ذلك، انخفضت كفاءة الحماية من النيوترونات السريعة بحوالي 24٪، مما يبرز اختلاف متطلبات المواد لتوهين أشعة غاما مقارنة بالنيوترونات. تؤكد هذه النتائج على إمكانات مركبات PVA لتوفير حماية إشعاعية مخصصة، مع تحقيق توازن بين التوهين لأشعة غاما والنيوترونات.

Abstract

This study investigates the effects of substituting cerium oxide (Ce_2O_3) with neodymium oxide (Nd_2O_3) in polyvinyl alcohol (PVA)-based composites on their structural, optical, and radiation shielding properties. Four composite films were synthesized via a solution casting method, with Nd_2O_3 concentrations ranging from 0 to 7.5 wt.%. The results revealed a

significant reduction in density (90.81%) for the highest Nd_2O_3-loaded sample (PCNd-75), attributed to enhanced polymer covalency and reduced packing efficiency. Gamma-ray shielding performance improved markedly, with mass attenuation coefficients increasing by 665% at 0.08 MeV and 11% at 2.614 MeV, driven by Nd_2O_3's higher atomic number (Z = 60) compared to Ce_2O_3 (Z = 58). However, neutron shielding efficiency decreased by approximately 24% for fast neutrons, highlighting divergent material requirements for gamma-ray versus neutron attenuation. These findings underscore the potential of PVA composites for tailored radiation shielding applications, balancing trade-offs between gamma and neutron attenuation.

Chapter 1: Introduction

Photon radiation, known for its penetrating capabilities, finds widespread use in various sectors. These include industrial applications, radiation protection, dosimetry, and medical fields like diagnostic imaging, therapeutic techniques, and sterilization protocols. As an indirect ionizing radiation, photons interact with the electrons of atoms and molecules within materials, leading to ionization and excitation. The extent of photon irradiation is quantified using radiation interaction parameters, such as mass attenuation coefficients and mass absorption coefficients. The following section provides a summary of the various ways gamma rays interact with matter.

1.1. Interactions of Photons with Matter

Photons are fundamental units of electromagnetic radiation, characterized by their lack of mass and electrical charge, and their propagation at the universal speed of light, c. A significant consequence of their neutrality is the absence of Coulombic interactions with atomic electrons, a mechanism through which charged particles typically lose energy. This unique property permits photons to traverse substantial paths within a medium before their energy is either partially or entirely imparted to electrons. The subsequent deposition of this energy in the material is governed by primary interaction processes: the photoelectric effect, Compton scattering, and pair production.

1.2. Photoelectric effect

The photoelectric effect describes an interaction where a photon is entirely absorbed by an atom. This absorption leads to the emission of an energetic photoelectron from one of the atom's tightly bound inner shells (K, L, or M). The total energy of the incoming photon (hv) is transferred to the ejected electron. This energy is then partitioned: some is used to overcome the electron's binding energy, and the rest becomes the kinetic energy of the liberated electron. The photoelectric process is the primary mechanism of photon interaction at relatively low photon energies and high atomic numbers (Z).

$$K.E = hv - b.e \tag{1.1}$$

The photoelectric process is the primary mechanism of photon interaction at relatively low photon energies and high atomic numbers (Z).

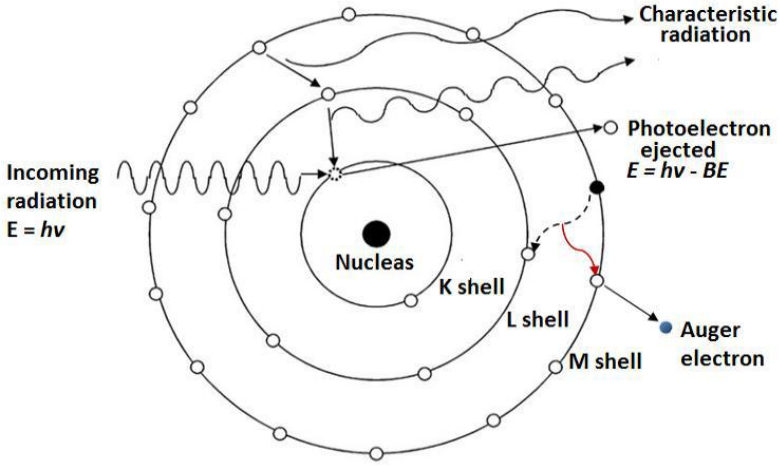

Figure 1.1: The photoelectric effect

1.3. Compton scatter

When high-energy photons interact with matter, exceeding the photoelectric effect threshold, electrons are emitted while the remaining photons are scattered. This particle-like interaction of photons with electrons. This interaction discovered by Arthur Holly Compton in 1923 at the University of Washington, the Compton Effect earned him the Nobel Prize in Physics in 1927. This phenomenon was crucial in demonstrating that light's behavior cannot be solely attributed to wave characteristics.

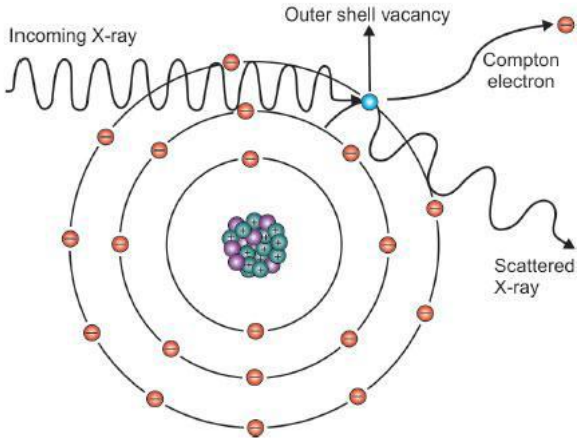

Figure 1.2: The Compton scattering

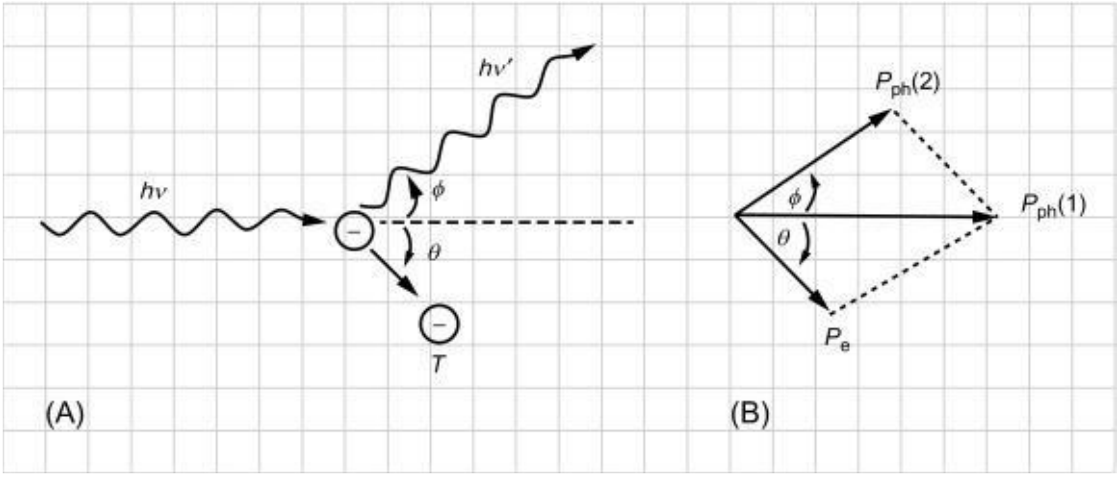

Figure 1.3: The Compton scattering

In Compton scattering, an incident photon interacts with a weakly bound electron, effectively treating it as "free" because its binding energy is negligible compared to the photon's energy. This interaction results in the electron being ejected and the photon being scattered, both at an angle θ, with the scattered photon experiencing a reduction in energy. Key characteristics of these interactions include: (1) all scattering angles are permitted, (2) the energy transferred to the electron can range from zero to a substantial portion of the gamma-ray energy, and (3) this mechanism is the most prevalent interaction in tissues for photon energies between 100 keV and 10 MeV. The likelihood of Compton scattering is nearly independent of the atomic number Z and decreases as the energy of the photon increases.

The relation between photon deflection and energy loss for Compton scattering is determined from the conservation of momentum and energy between the photon and the recoiling electron. This relation can be expressed as:

$$h\nu = \frac{h\nu_0}{1+\left(\frac{h\nu_0}{m_e c^2}\right)(1-cos\theta)}, \quad (1.2)$$

$$T = h\nu_0 - h\nu \quad (1.3)$$

Where $h\nu_0$ is the energy of incident photon, $h\nu$, is the energy of scattered photon, E is the energy of recoil electron, m_e is the rest mass of an electron, and c is the speed of light.

1.4. Pair Production

When a photon with energy exceeding 1.022 MeV interacts with matter, it can undergo **pair production**. As the photon passes near an atomic nucleus, the strong electromagnetic field of the nucleus facilitates the conversion of the photon's energy into an electron-positron pair (e^- and e^+). The original photon disappears, and its energy is transformed into the rest mass of the two particles (2 × 0.511 MeV = 1.022 MeV) plus their kinetic energy. Any excess energy beyond the 1.022 MeV threshold is distributed as kinetic energy between the newly created particles.

$$E_{e^+} + E_{e^-} = h\nu - 1.022 \text{ (MeV)} \quad (1.2)$$

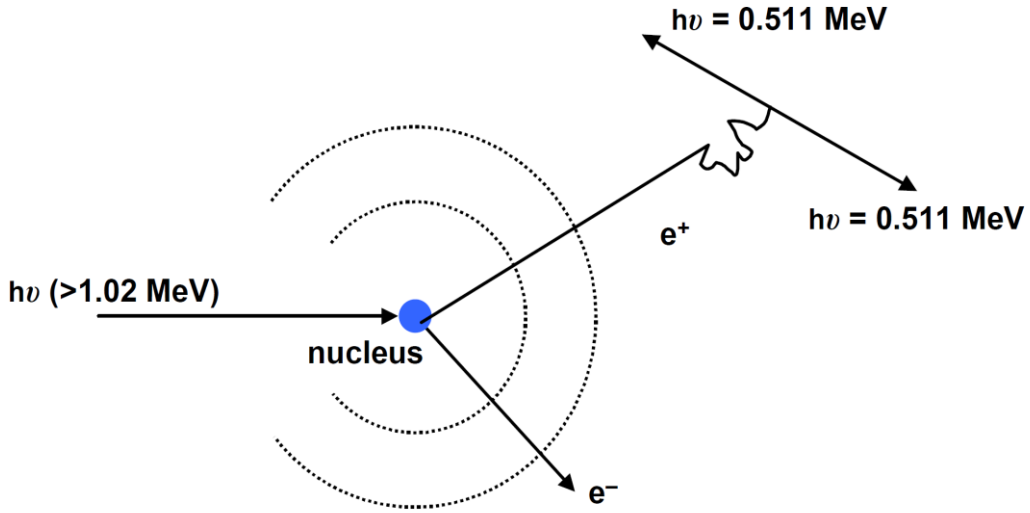

Figure 1.3: The pair production process.

Photon interactions with matter vary significantly with energy, with distinct processes dominating specific energy ranges. The photoelectric effect prevails at lower energies, Compton scattering around 1 MeV, and pair production at higher energies. The relative interaction probability quantifies the likelihood of each process occurring at a given energy.

Understanding these probabilities is crucial for applications such as medical imaging and radiation therapy. The dominant interaction—whether coherent scattering, photoelectric absorption, Compton scattering, or pair production—depends on photon energy and material properties. These probabilities are derived from attenuation

coefficients and cross-sections, often computed using tools like *XCom* ((Gerward et al., 2004)., 2001) and NXCom (El-Khayatt, 2011).

1.5. Litrutre reviwe

Polyvinyl pyrrolidone (PVP) is widely used in various industries due to its strong environmental stability, processability, and good electrical conductivity. Meanwhile, PVA composites incorporating inorganic oxides exhibit hybrid crystalline/amorphous structures, synergizing the properties of both components. These composites can complex with metal cations, enhancing their performance in electrochemical devices, displays, and photovoltaic cells, while remaining easily processable into thin films. By blending polymers, composites with customized functionalities can be engineered for specific applications (Abdelrazek et al., 2010; Elashmawi and Abdel Baieth, 2012; Ragab, 2011).

PVA's high transparency and adjustable refractive index render it particularly suitable for optical applications, including films, lenses, and waveguides. Its minimal light absorption ensures precise light management in filters and optical windows.

Nd_2O_3 and Ce_2O3 have distinct optical properties: Nd_2O_3 absorbs infrared, useful for filters and lasers in medicine/environment, blocking UV but opaque in visible light. CeO_2 absorbs UV-visible light, used in UV-blocking, polishing, and catalysts, with transparency exceeding Nd_2O_3 based on structure/size. Nd_2O_3's wide infrared band gap lowers visible transparency; CeO_2's narrower gap enables UV-visible absorption/transmission. Research focuses on rare earth oxide substitution in PVA for optical applications (Aguiar et al., 2020; and Zulkipli et al., 2023).

1.6. Aim of the work

This study explores how substituting Ce_2O_3 with Nd_2O_3 in PVA-Ce_2O_3 composites affects their structure and shielding effectiveness against gamma rays and neutrons.

Chapter 2: Material and methods

2.1. Sample Preparation

The low-cost casting process was employed to create polymer composite samples with the following chemical compositions: 65 wt. % PVA $(C_2H_4O)_n$ + (35-*x)* wt. % Ce_2O_3, + *x* wt. % Nd_2O_3, where *x* = 0, 2.5, 5, and 7.5 wt.%. PVA was synthesized through solution casting using a magnetic stirrer at 60 °C for 3 hours until a homogeneous, transparent solution was achieved. The PVA/Ce_2O_3 /Nd_2O_3 polymer composite samples were prepared by incorporating the appropriate weight fractions of the salts into the polymer blend solutions, with Ce and Nd cations uniformly dispersed via ultrasonic mixing. Homogeneous mixtures were poured onto flat Petri plates and allowed to dry at room temperature for several days, after which the films were cut into 2 x 2 cm^2 sections. Four compositions with varying Nd (0 -7.5 wt.%) were obtained, labeled as PCNd-00, PCNd-25, PCNd-50, and PCNd-75, corresponding to Nd_2O_3 loadings in PVA/Ce_2O_3 (65/35).

Table 2.1: Density values of glass samples

Sample Code	*x*%	Composition	ρ(g/cm^3)
PCNd-00	0	65 PVA-35Ce_2O_3	2.097
PCNd-25	2.5	65 PVA-32.5 Ce_2O_3-2.5Nd_2O_3	1.92
PCNd-50	5	65 PVA-30 Ce_2O_3-5Nd_2O_3	1.859
PCNd-75	7.5	65 PVA-27.5 Ce_2O_3-7.5Nd_2O_3	1.691

Table 2.2: Chemical composition(wt.%) and mol %of the composite samples

Sample	Compound	Molar mass	wt. (%)	mol (%)
PCNd-00	C_2H_4O	28.634	65	19.95
	Ce_2O_3	114.881	35	80.05
PCNd-25	C_2H_4O	28.634	65	19.92
	Ce_2O_3	106.675	32.5	74.22
	Nd_2O_3	8.412	2.5	5.85
PCNd-50	C_2H_4O	28.634	65	19.89
	Ce_2O_3	98.469	30	68.42
	Nd_2O_3	16.824	5	11.69
PCNd-75	C_2H_4O	28.634	65	19.87
	Ce_2O_3	90.263	27.5	62.62
	Nd_2O_3	25.236	7.5	17.51

2.2. Theoretical calculations

The attenuation of x-rays and gamma rays in a material can commonly be expressed using the exponential attenuation law. The basic equation is given by(El-Khayatt, 2017):

$$I = I_o e^{-\mu x} \quad (2.1)$$

Where:

I_o is the intensity (or number of photons) after passing through a distance x in the material,

I_o is the initial intensity (or number of photons) of the beam before entering the material,

μ is the linear attenuation coefficient of the material, which is a measure of how strongly the material can attenuate the beam through various interactions (including Compton scattering, photoelectric absorption, and pair production),

x is the thickness of the material that the photons are traveling through.

The linear attenuation coefficient (μ) can be considered as a combination of several contributions from different types of interactions. Each type of interaction contributes to the overall attenuation depending on the energy of the photons and the properties of

the material. Further elaboration on the specific contributions to μ can be provided by separating it into relevant components(El-Khayatt, 2011):

$$\mu = \mu_{\text{coh}} + \mu_{\text{com}} + \mu_{\text{photo}} + \mu_{\text{pair}} \quad (2.2)$$

Where:

- μ_{coh} is the contribution from coherent (Rayleigh) scattering,

- μ_{com} is the contribution from Compton scattering,

- $\mu_{\text{photo}}$is the contribution from the photoelectric effect,

- $\mu_{\text{pair}}$is the contribution from pair production.

In this work, the partial interaction probability is calculated by dividing each partial contribution by μ.

In a narrow beam of monoenergetic photons, each Compton scattering event removes a photon from the beam, much like absorption does. These interactions contribute to the overall attenuation, dictating how the beam's intensity diminishes as it passes through matter. This exponential attenuation is a fundamental principle in medical imaging, radiation protection, and materials science.

The mass attenuation coefficient (μ_m, measured in cm^2/g) quantifies a material's ability to attenuate (weaken) radiation intensity per unit mass. This parameter is particularly valuable in fields such as medical imaging and radiation shielding, as it enables direct comparisons of how different materials interact with various radiation types based on their mass rather than their volume.

Mathematically, the mass attenuation coefficient is defined as the linear attenuation coefficient (μ) divided by the absorber's density (ρ, in g/cm^3):

$$\mu_m = \mu/\rho \quad (2.3)$$

where:

ρ is the density of the absorber (in g/cm^{-3}).

The mass attenuation coefficients of compounds and mixtures—such as glass, concrete, and composites—can be computed using specialized software tools like NXcom (El-

Khayatt, 2011)and WinXCom (Gerward et al., 2001). NXcom, developed by El-Khayatt, calculates fast neutron attenuation coefficients along with total and partial photon interaction cross-sections, encompassing absorption and scattering processes. In contrast, WinXCom, created by Gerward et al., determines the gamma-ray mass attenuation coefficient (μ_m, cm^2/g). Both programs rely on the mixture rule, which posits that the total attenuation is the sum of the individual contributions from each constituent, as expressed in the following equations :

$$(\mu_m)_{sample} = \sum_i w_i \, (\mu_m)_i \tag{2.4}$$

Here ρ_i denotes the density of the i^{th} constituent element in the sample, while w_i represents the weight fraction. The weight fraction of an element in a compound is found from

$$w_i = k_i A_i \, / A \tag{2.5}$$

where k_i is the number of i^{th} atoms of the i^{th} element, and A is the molecular weight of the compound.

Table 2.3: Equations used to determine gamma-ray and neutron shielding parameters.

Parameter	Symbol	Unit	Equation	Explanation
Linear attenuation coefficient (LAC)	μ	cm^{-1}	$\mu = -\frac{1}{x} ln(I/I_0)$	x: sample thickness (cm or $g.cm^{-2}$) I_0(incident) and I(transmitted) photon intensities.
Mass attenuation coefficient (MAC)	μ_m	cm^2/g		
Removal neutron cross section of fast neutron	Σ_R	cm^{-1}	$\Sigma = -\frac{1}{x} ln(\phi/\phi_0)$	ϕ_0(incident) and ϕ (transmitted) neutron fluxes.
Half-value layer	HVL	cm	$HVL \; ln2/\Sigma; \; ln2/\mu$	Distance for intensity to drop to half.
Relaxation Length	λ	cm	$\lambda = 1/\Sigma; \; 1/\mu$	Distance for intensity to drop to 1/e (~36.8%).

Chapter 3: Results and discussion

3. Radiation shielding parameters

3.1. Gamma-ray characteristics

Table 3.1 displays the gamma-ray attenuation properties of the synthesized polymer composites across seven energy levels, covering low, medium, and high ranges using various radioisotopes. The table compares experimental and computational (XCOM) mass attenuation coefficients (μ_m), revealing a strong correlation between the two, with excellent agreement observed at all energies. The mass attenuation coefficient decreases as energy increases, attributed to declining photoelectric absorption and rising Compton scattering dominance.

Composites incorporating Nd_2O_3 consistently exhibit higher μm values than their neodymium-free counterparts. Notably, a 7.5 wt.% Nd_2O_3 addition increases μm by approximately 665% at 0.08 MeV and 11% at 2.614 MeV, underscoring its significant role in enhancing radiation shielding. Furthermore, each 1 wt.% increment of Nd_2O_3 improves shielding efficiency beyond its proportional weight contribution, indicating a synergistic effect. This enhancement stems from the higher atomic number of neodymium (Nd, Z = 60) compared to cerium (Ce, Z = 58), leading to superior photon interaction.

In Figure 3.1, the highest linear attenuation coefficients (μ) at 0.08 MeV are 4.36, 2.88, 1.54, 0.97, and 0.46 cm^{-1} for PCNd-75 to PCNd-00, respectively. Beyond this energy, the μ values decline sharply with increasing photon energy across all samples. Above 0.238 MeV, the curves begin to converge, as the Compton scattering (CS) process—

dominant in this region—is less sensitive to atomic number compared to the photoelectric effect (PE).

Table 3.1: XCom calculated values of mass attenuation coefficients, and the percentage improvement of the PCNd-75 sample relative to the PCNd-00 sample.

Sample	E (MeV)						
	0.08	0.238	0.356	0.662	1.173	1.333	2.614
PCNd-00	0.2721	0.1618	0.1358	0.1001	0.0711	0.0607	0.0402
PCNd-25	0.2721	0.1618	0.1358	0.1001	0.0711	0.0607	0.0402
PCNd-50	1.4124	0.221	0.1566	0.1056	0.0734	0.0674	0.0428
PCNd-75	2.0746	0.258	0.1728	0.1112	0.0765	0.0699	0.0447
Improvement†	664.7	59.6	27.5	11.2	7.6	15.3	11.3

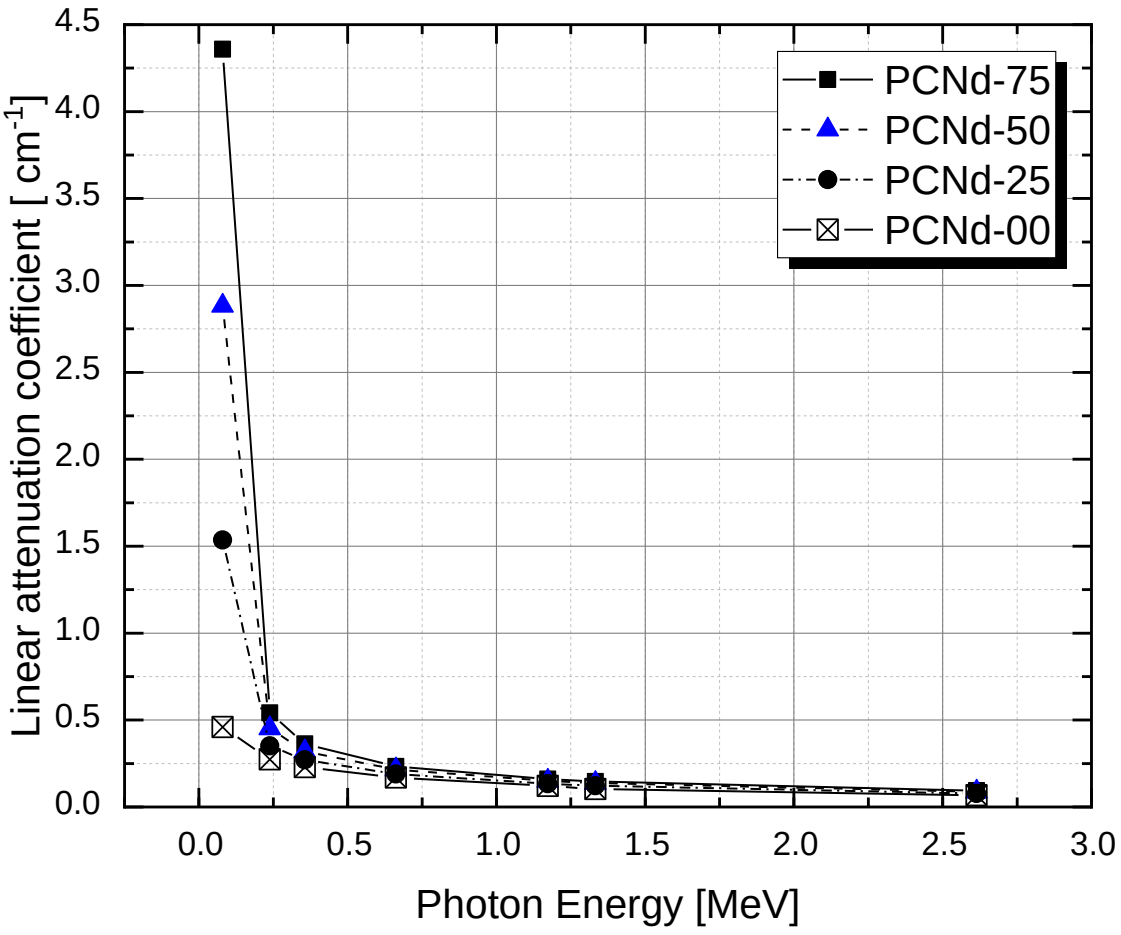

Figure 3. 1: Linear attenuation coefficients of photons in the studied samples.

Figures 3.2(a) and 3.2(b) display the measured HLV and λ values of the polymer composites, which demonstrate an inverse correlation with the material's attenuation capability. As the Nd_2O_3 content increases, these parameters decrease, resulting in enhanced attenuation performance. The HLV and λ values follow a consistent trend across the samples, with the lowest values observed in the order: PCNd-75 < PCNd-50 < PCNd-25 < PCNd-00. Notably, the HLV values are consistently lower than λ, where λ represents the mean free path—the thickness required to reduce radiation intensity to 37% of its initial value, as depicted in Figure 3.2.

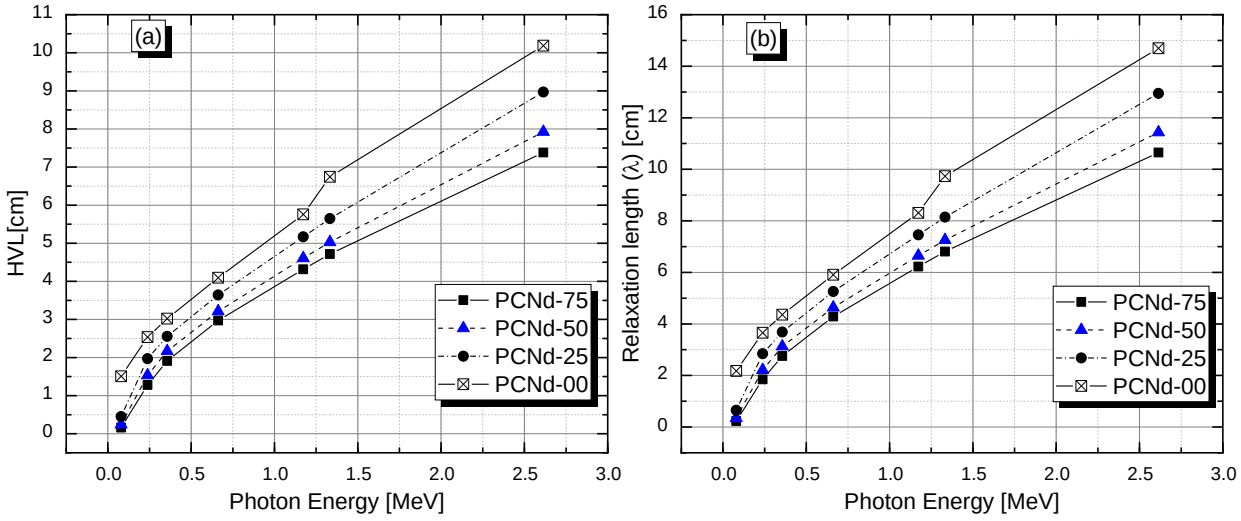

Figure 3. 2: Half-value layer (**a**), relaxation length (**b**) determined for gamma-ray.

3.2. Fast neutron attenuation

When a fast neutron collides with hydrogen, it loses a substantial amount of energy, effectively removing it from the beam. This phenomenon allows neutron attenuation to be modeled as a "removal process." The removal cross-section (denoted as Σ_R in cm^{-1}) quantifies neutron attenuation and represents the probability of large-angle scattering events—whether elastic or inelastic—that are likely to eject the neutron from the beam. Several programs, such as NXcom, developed by Elkhayatt in 2011, have been created to compute the removal cross-section (Σ_R) of compounds or homogeneous mixtures.

These calculations rely on the removal cross-sections of the individual components and follow the mixture rule, expressed as:

$$\Sigma_R = \sum_i \rho_i (\Sigma_R/\rho)_i \quad (3.1)$$

Here, ρ_i represents the partial density (the density of the ith constituent within the mixture), and $(\Sigma_R/\rho)_i$ denotes the mass removal cross-section of the ith constituent.

Table 3.2 summarizes the fast neutron removal cross-section for various compositions with different Nd_2O_3 ratios. While the mass removal cross-section of Nd_2O_3 (0.01641 cm^2/g) is marginally lower than that of Ce_2O_3 (0.01668 cm^2/g), the results indicate that increasing the Nd_2O_3 content reduces fast neutron removal efficiency. This reduction is primarily due to the lower density caused by substituting Ce_2O_3 with Nd_2O_3, which decreases neutron interactions per unit penetration length. As shown Table 1.2, the control sample exhibits a 90.81% higher density and a 35.48% greater removal cross-section compared to the PCNd-75 sample.

Table 3.2: Fast neutron cross-section and relaxation length in the studied samples

Sample	Σ_R, cm^{-1}	λ, cm
PCNd-00	0.14416	6.94
PCNd-10	0.14046	7.12
PCNd-25	0.13202	7.57
PCNd-50	0.12783	7.82
PCNd-75	0.11628	8.60

4. Conclusions

This study demonstrates that substituting Ce_2O_3 with Nd_2O_3 in PVA-Ce_2O_3 composites significantly alters their structural, optical, and radiation shielding properties. The key observations are as follows:

1. **Density Reduction:** The PCNd-75 composite exhibited a 90.81% decrease in density compared to the control (PCNd-00), attributed to enhanced polymer covalency and reduced packing efficiency.
2. **Gamma-Ray Shielding Performance:** Gamma-ray attenuation results showed excellent agreement, with shielding efficiency improving by 665% at 0.08 MeV and 11% at 2.614 MeV compared to the control.
3. **Neutron Shielding Behavior:** Incorporating 7.5 wt.% Nd_2O_3 reduced fast and thermal neutron shielding (Σ_R) by ~24% compared to the Nd_2O_3-free sample.
4. The **opposite behavior** of neutron shielding **highlights** a divergence from gamma-ray shielding trends, emphasizing the distinct material requirements for neutron versus gamma attenuation.

References

Abdelrazek, E.M., Elashmawi, I.S., El-khodary, A., Yassin, A., 2010. Structural, optical, thermal and electrical studies on PVA/PVP blends filled with lithium bromide. Current Applied Physics 10, 607–613. https://doi.org/10.1016/j.cap.2009.08.005

Aguiar, L.W., Botero, E.R., Carvalho, C.T., Caires, A.R.L., da Silva, C.T.P., Rinaldi, A.W., Guo, R., Bhalla, A.S., Falcao, E.A., 2020. Study of the changes in the polar phase and optical properties of poly (vinylidene fluoride) matrix by neodymium compound addition. Mater Today Commun 25. https://doi.org/10.1016/j.mtcomm.2020.101274

Elashmawi, I.S., Abdel Baieth, H.E., 2012. Spectroscopic studies of hydroxyapatite in PVP/PVA polymeric matrix as biomaterial. Current Applied Physics 12, 141–146. https://doi.org/10.1016/j.cap.2011.05.011

El-Khayatt, A.M., 2017. Semi-empirical determination of gamma-ray kerma coefficients for materials of shielding and dosimetry from mass attenuation coefficients. Progress in Nuclear Energy 98, 277–284. https://doi.org/10.1016/j.pnucene.2017.04.006

El-Khayatt, A.M., 2011. NXcom – A program for calculating attenuation coefficients of fast neutrons and gamma-rays. Ann Nucl Energy 38, 128–132. https://doi.org/10.1016/j.anucene.2010.08.003

Esro, M., Kolosov, O., Stolojan, V., Jones, P.J., Milne, W.I., Adamopoulos, G., 2017. Solution-Processed Neodymium Oxide/ZnO Thin-Film Transistors with Electron Mobility in Excess of 65 cm V−1 s−1. Adv Electron Mater 3. https://doi.org/10.1002/aelm.201700025

Gerward, L., Guilbert, N., Bjørn Jensen, K., Levring, H., 2001. X-ray absorption in matter. Reengineering XCOM. Radiation Physics and Chemistry 60, 23–24. https://doi.org/10.1016/S0969-806X(00)00324-8

Gerward, L., Guilbert, N., Jensen, K.B., Levring, H., 2004. WinXCom—a program for calculating X-ray attenuation coefficients. Radiation Physics and Chemistry 71, 653–654. https://doi.org/10.1016/j.radphyschem.2004.04.040

Keikhaei, M., Motevalizadeh, L., Attaran-Kakhki, E., 2016. Optical properties of neodymium oxide nanoparticle-doped polyvinyl alcohol film. Int J Nanosci 15. https://doi.org/10.1142/S0219581X16500125

Ragab, H.M., 2011. Spectroscopic investigations and electrical properties of PVA/PVP blend filled with different concentrations of nickel chloride. Physica B Condens Matter 406, 3759–3767. https://doi.org/10.1016/j.physb.2010.11.030

Tatar, B., Gökdemir, F.P., Pehlivan, E., Urgen, M., 2013a. The influence of Er3+ doping on the structural and optical properties of CeO2 thin films grown by PED. Appl Surf Sci 285, 409–416. https://doi.org/10.1016/j.apsusc.2013.08.068

Tatar, B., Gökdemir, F.P., Pehlivan, E., Urgen, M., 2013b. The influence of Er 3+ doping on the structural and optical properties of CeO 2 thin films grown by PED. Appl Surf Sci 285. https://doi.org/10.1016/j.apsusc.2013.08.068

Yang, Y., Du, X., Yi, C., Liu, J., Zhu, B., Zhang, Z., 2018. Structural, optical and electrical properties of CeO 2 thin films simultaneously prepared by anodic and cathodic electrodeposition. Appl Surf Sci 440. https://doi.org/10.1016/j.apsusc.2018.01.179

Zulkipli, N.F., Beh, C.Y., Teng, H.C., Muhammad, A.R., Rosol, A.H.A., Yusoff, R.A.M., Ahmed, N., Omar, S., Yasin, M., Harun, S.W., 2023. Neodymium oxide saturable absorber for generating Q-switched and mode-locked pulses in 1.55-micron region. Optik (Stuttg) 293. https://doi.org/10.1016/j.ijleo.2023.171410